



Published in final edited form as:

Nature. 2022 October ; 610(7931): 389–393. doi:10.1038/s41586-022-05278-9.

## NMR-Guided Directed Evolution

Sagar Bhattacharya<sup>1</sup>, Eleonora G. Margheritis<sup>2</sup>, Katsuya Takahashi<sup>2</sup>, Alona Kulesha<sup>1</sup>, Areetha D'Souza<sup>1</sup>, Inhye Kim<sup>1</sup>, Jennifer H. Yoon<sup>1</sup>, Jeremy R. H. Tame<sup>2</sup>, Alexander N. Volkov<sup>3,4,\*</sup>, Olga V. Makhlynets<sup>1,\*</sup>, Ivan V. Korendovych<sup>1,\*</sup>

<sup>1</sup>Department of Chemistry, Syracuse University, 111 College Place, Syracuse, NY 13244, USA.

<sup>2</sup>Graduate School of Medical Life Science, Yokohama City University, 1-7-29 Suehiro, Yokohama, Kanagawa 230-0045, Japan.

<sup>3</sup>VIB Centre for Structural Biology, Vlaams Instituut voor Biotechnologie (VIB), Pleinlaan 2, Brussels, 1050 Belgium

<sup>4</sup>Jean Jeener NMR Centre, Vrije Universiteit Brussel (VUB), Pleinlaan 2, Brussels, 1050 Belgium.

Directed evolution is a powerful tool for improving existing properties and imparting completely new functionalities onto proteins.<sup>1–4</sup> Nonetheless, even in small proteins its potential is inherently limited by the astronomical number of possible amino acid sequences. Sampling the complete sequence space of a 100-residue protein would require testing of  $20^{100}$  combinations, which is currently beyond any existing experimental approach. Fortunately, in practice, selective modification of relatively few residues is sufficient for efficient improvement, functional enhancement and repurposing of existing proteins.<sup>5</sup> Moreover, computational methods have been developed to predict the location, and, in certain cases, identities of potentially productive mutations.<sup>6–9</sup> Importantly, all current approaches for prediction of hot spots and productive mutations rely heavily on structural information and/or bioinformatics, which is not always available for proteins of interest. Moreover, they offer limited ability to identify beneficial mutations far from the active site, even though such changes may dramatically improve the catalytic properties of an enzyme.<sup>10</sup> Machine learning methods have recently showed promise in predicting productive mutations,<sup>11</sup> yet they often require large high quality training data sets which are hard to obtain in directed evolution experiments. Here we show that mutagenic hot spots in enzymes can be identified using Nuclear Magnetic Resonance (NMR) spectroscopy. In a proof-of-concept study, we converted myoglobin, a non-enzymatic oxygen storage protein, into a highly efficient Kemp eliminase using only three mutations. The observed levels of catalytic efficiency ( $k_{\text{cat}}/K_M$  of  $1.6 \times 10^7 \text{ M}^{-1}\text{s}^{-1}$  and  $k_{\text{cat}}/k_{\text{uncat}} > 10^8$ ) are the highest

\* Corresponding author. ikorendo@syr.edu, ovakhly@syr.edu, ovolkov@vub.be. **Correspondence and requests for materials** should be addressed to Ivan V. Korendovych.

**Author contributions** I.V.K., O.V.M. and A.N.V. designed the experiments. S.B., A.K., J.H.Y. and I.K. performed directed evolution, protein expression and characterization as well as kinetic studies. A.D., A.N.V., O.V.M. and I.V.K. performed NMR titrations, backbone and side chain assignment and NMR data analysis. E.M., K.T. and J.R.H.T. expressed and crystallized the proteins and solved their structures. I.V.K. and O.V.M. wrote the manuscript with input of all the authors. These authors contributed equally to this work: Eleonora Margheritis, Katsuya Takahashi, Alona Kulesha

**Competing interests** The authors declare that they have no competing interests.

Additional information

**Supplementary information** The online version contains supplementary material available at <https://doi.org/>

reported for any designed protein and are on par with the levels shown by natural enzymes for the reactions they are evolved to catalyze. Given the simplicity of this experimental approach, which requires no *a priori* structural or bioinformatic knowledge, we expect it to be widely applicable and to unleash the full potential of directed enzyme evolution.

Recent paradigm shifting advances in understanding the fundamental principles that drive enzyme evolution point to a major role of global conformational selection for productive arrangements of functional groups to perfect transition state stabilization, as well as steric and electrostatic interactions<sup>12–16</sup>. Here we seek to build on this recent work to predict experimentally the locations of the productive mutations that can minimize non-essential protein dynamics to achieve high catalytic efficiency. Efficient catalysis relies on tight and specific association of the substrate with the enzyme, placing it in a unique anisotropic environment (often with a high dipole moment, considered to be important for activity<sup>17</sup>). Experimentally, such an environment can be evaluated using NMR, which provides residue-level information under catalytic conditions without the need for full structural characterization. In a conformational ensemble, residues that require substantial reorganization to adopt or to increase the population of a specific rotamer to support the transition state should experience a large change in their NMR chemical shift upon addition of the corresponding transition state analog (usually a competitive inhibitor). Thus, analysis of the chemical shift perturbation (CSP) upon inhibitor addition may help identify mutagenic hot spots in the protein structure, both near and far from the active site.

Kemp elimination (Fig. 1) is a well-established and benchmarked model reaction for testing protein design and evolution methodologies<sup>18–26</sup>. Inspired by the recent discovery of redox-mediated Kemp elimination promoted by cytochrome P450<sup>27</sup> and aldoxime dehydratases<sup>28</sup>, we set out to explore whether an NMR-guided approach can be successfully used to evolve a novel Kemp eliminase from a non-enzymatic heme protein. For an unbiased test of the approach, we chose not to perform any computational pre-selection of possible candidates, but rather focused on the simplest proteins. Myoglobin (Mb), arguably the most well-characterized heme protein, adopts catalytic functionalities upon replacement of distal histidine His64<sup>29</sup>, which in the native protein controls oxygen binding and slows heme oxidation. Mb-H64V has been extensively studied before<sup>30</sup>, so we experimentally tested this mutant for the ability to promote Kemp elimination. In the reduced form, Mb-H64V demonstrated catalytic efficiency of  $255 \text{ M}^{-1}\text{s}^{-1}$  at pH 8.0 presenting itself as a promising candidate for NMR-guided directed evolution (Table 1). Even with paramagnetism and high helical content of the reduced protein, a nearly full backbone assignment was possible, which enabled us to perform a CSP study using 6-nitrobenzotriazole (6-NBT), an inhibitor of Kemp elimination (Fig. 1). The data show 15 hot spots, defined as regions with residue CSP Z-scores of above *ca.* 1, dispersed around the protein, both near to and away from the heme cofactor (Fig. 2a,d). Next, we prepared saturation mutagenesis libraries in all positions with  $Z \geq 1$  and their immediate neighbors (except for the proximal His93 that was not considered as it is required for the heme cofactor binding). Crude lysate screening of the saturation mutagenesis libraries showed hits in all hot spots. Purification of the identified proteins confirmed the screening results in all cases (with increases in catalytic efficiencies ranging from 2-fold to 72-fold, with an average of 20-fold) except in one instance (Mb-H64V/Q152M), where we were unable to produce enough soluble protein for

kinetic characterization. Nine of the 19 identified productive mutations were located away from the active site (Fig. 2d).

Saturation mutagenesis performed in 18 randomly selected positions with small CSP yielded no hits (Fig. 2a, blue asterisks). Since the probability of finding productive mutations is highest close to the active site, we have sampled all cold spots in the immediate vicinity of the active site and tried to provide a representative sampling of the positions located further away (Extended Data Fig. 1). In a subsequent non-exhaustive gene shuffling experiment, we found that L29I, H64G and V68A can be productively combined with positive synergy (the triple mutant is 3-fold more active than predicted from the three individual mutations), a trait quite uncommon in traditional directed evolution experiments. The resulting enzyme Mb-L29I/H64G/V68A, named FerrEiCat for FERRous Kemp ELimination CATalyst, showed a remarkable Kemp elimination activity with catalytic efficiency of  $15,721,000 \text{ M}^{-1}\text{s}^{-1}$  at pH 8 (Table 1). This level of catalytic efficiency is almost two orders of magnitude higher than that of the most active reported Kemp eliminase HG3.17, evolved in 17 rounds of directed evolution<sup>20</sup>, and is on par with the levels shown by natural enzymes for the reactions they have evolved to catalyze, being just 1–2 orders of magnitude from the diffusion limit. Importantly, the NMR-guided approach yields mutants with high  $k_{\text{cat}}$  values ( $3,656 \text{ s}^{-1}$  for FerrEiCat), a trait that is often hard to achieve in traditional approaches to directed evolution, where high levels of catalytic efficiency are often achieved by lowering the  $K_{\text{M}}$ . FerrEiCat is capable of at least 10,000 turnovers before showing signs of product inhibition (Extended Data Fig. 2). The unprecedented, experimentally guided *ca.* 62,000-fold improvement in catalytic efficiency (Extended Data Fig. 3) over the starting design was obtained with only three mutations in a non-enzymatic protein (Fig. 2c). The crystal structure of FerrEiCat shows remarkable similarity to the starting point of the evolution<sup>31</sup> (backbone RMSD of 0.16 Å, Fig. 2e) and the newly introduced mutations had only minor effect on the cofactor redox potential (Extended Data Fig. 4). While we were unable to obtain a crystal structure of FerrEiCat with an inhibitor, docking studies (Fig. 2e) show that directed evolution results in the creation of a tight binding pocket bringing the substrate into proximity to the heme iron. Strikingly, we were unable to dock either 5-NBI or 6-NBT into the crystal structure of Mb-H64V, since computationally predicted binding pocket is too small (Fig. 2d). Yet, CSP analysis clearly shows association of the inhibitor with the protein, highlighting the power of NMR to readily identify productive arrangements of molecules that may not be apparent in modelling based on static crystal structures.

To test the general applicability of the NMR-guided directed evolution we applied it to the Kemp eliminases of the AlleyCat family that promote benzisoxazole ring opening using base-facilitated catalysis.<sup>18–24</sup> AlleyCat was designed using a minimalist approach by introducing a single glutamate residue into the 74-residue C-terminal domain of calmodulin (cCaM), a non-enzymatic protein<sup>32</sup>. Subsequently, in seven rounds of directed evolution using saturation mutagenesis, error-prone PCR (epPCR) and gene shuffling, we evolved AlleyCat into AlleyCat7, which showed turnover numbers on par with some of the best examples of Kemp eliminases.<sup>33</sup> Due to its small size, diamagnetism, extensive previous characterization, and a wealth of functional data obtained through traditional approaches to directed evolution, the AlleyCat proteins provide an excellent and unbiased test-bed for the NMR-guided directed evolution both retrospectively, to evaluate the performance of

CSP based approaches, and prospectively to test the limits of the method. CSP maxima observed upon titrating 6-NBT into the C-terminal domain of calmodulin that was used as a starting point of the design (Fig. 3a) are in excellent agreement with the first three mutations introduced into the protein during the design and subsequent directed evolution<sup>33</sup>: F92E, M144R and H107I. Residue 107 is notably not part of the substrate binding pocket. Upon introduction of the F92E mutation, a new hot spot consistent with the previously found productive A88Q mutation in AlleyCat appears (Fig. 3a). Interestingly, we observed a drop in CSP Z-values in the C-terminal region of the protein, where beneficial mutations in positions 144 and 145 were found in AlleyCat, potentially related to a more than 3-fold drop in affinity for the inhibitor ( $K_d$  of 3.3 mM for AlleyCat vs. 1.0 mM for cCaM). Encouraged by the similarity between the traditional and NMR-guided evolution trajectories, we undertook a prospective study to determine whether CSP analysis could be used to improve the catalytic efficiency of AlleyCat7. The CSP data for AlleyCat7 (Fig. 3b) are quite different from those of cCaM and AlleyCat both in terms of positions of the major peaks as well as their relative magnitude. We chose not to pursue residues in the calcium-binding EF-hand domains that are essential for both the fold and allosteric regulation. Since we have already introduced mutations at positions 124, 128 and 144, we performed saturation mutagenesis at position 125. AlleyCat7-I125H (named AlleyCat8) identified in the screening showed a 3-fold increase in  $k_{cat}$  (Table 1). No beneficial mutations were found by saturation mutagenesis studies of any positions that did not show significant CSP (Fig. 3b, blue asterisks). The CSP graph for AlleyCat8 again shows significant changes (Fig. 3c). The most prominent shifts for AlleyCat8 are observed for residues 114–116, which were little affected in previous generations of the protein, as well as residues 143 and 146. Saturation mutagenesis in positions 114, 115, 116 and 146 (position 143 is next to the previously mutated Met144) yielded productive mutations K115P (a variant subsequently called AlleyCat9) and T146R, showing significant improvements in  $k_{cat}/K_M$ , driven by the increase in  $k_{cat}$  for the former and the decrease in  $K_M$  for the latter. The effect of these two mutations is additive, so that the resulting protein AlleyCat10 shows  $k_{cat}/K_M$  of 4,378  $M^{-1}s^{-1}$ , and  $k_{cat}$  of 21.0  $s^{-1}$ . This represents a 750-fold improvement in catalytic efficiency over the starting design (a value second only to that shown by FerrE1Cat, Extended Data Fig. 3) that was achieved almost exclusively by improving  $k_{cat}$ .

The new members of the AlleyCat family fully preserve allosteric regulation by calcium (Extended Data Fig. 5). Crystallographic characterization of AlleyCat9 and AlleyCat10 both in the absence and in the presence of the inhibitor shows that these highly evolved variants, having more than 10% of their sequence mutated, remain structurally very similar (backbone RMSD 0.6–0.9 Å) to the C-terminal domain of calmodulin that served as a basis for the design (Fig. 3e,f).<sup>34</sup> Two of the three newly introduced productive mutations, Pro115 and Arg146, are located away from the active site ( $> 10$  Å from the inhibitor), showing the practical utility of CSP patterns to identify effectively mutagenic hot spots across the whole protein. Analysis of the difference in crystallographic B-factors in the crystal structures of the apo and the inhibitor bound AlleyCat9 (Fig. 3c) shows significant rigidification of the protein structure upon binding of the transition state analog, consistent with the contribution of protein dynamics to the observed CSP patterns.

In conclusion, we have discovered a strong correlation between the degree of NMR CSP of backbone amide resonances in  $^{15}\text{N}$ - $^1\text{H}$  HSQC spectra of enzymes by an inhibitor and the probability of finding a beneficial mutation in the vicinity of that residue. The chemical shift perturbation maps are highly sensitive to minor changes in protein sequences and pinpoint areas likely to affect catalytic activity, even if located far from the active site. In a proof-of-concept study, we converted myoglobin, a non-enzymatic oxygen storage protein, into a highly efficient Kemp eliminase using only three mutations. To our knowledge, this represents the first example of an experimental approach to guide directed evolution that does not rely on *a priori* structural or bioinformatic analyses, and only requires reliable backbone amide assignments and an appropriate inhibitor. Such NMR data can usually be easily obtained for soluble, folded proteins with fewer than about 300 residues, a criterion that is true for many enzymes selected for directed evolution. Given the simplicity of this experimental approach, which we applied successfully to two unrelated proteins that utilize different mechanisms, we expect the CSP-guided methodology to be widely applicable to other proteins and unleash the full potential of directed evolution to rapidly create new enzymes for practically important chemical transformations. These results also highlight the power of the minimalist approach to design of protein catalysts<sup>35</sup>, which allows for quick and inexpensive identification of starting points for subsequent directed evolution without detailed consideration of the reaction mechanism as well as extensive computation, and instead exploits the incredible plasticity of proteins to adopt new functions. Last but not least, our results contribute to the ongoing debate about the role of dynamics in enzymatic catalysis<sup>12–16</sup> by prospectively validating the importance of conformational flexibility in protein evolution. This opens the path to new fundamental studies of enzymatic function and evolution.

## Methods

### Chemicals and reagents

Reagents and buffers were purchased from Biobasic, Inc. and Santa Cruz Biotechnology, Inc. Buffers were made using MilliQ water (Millipore Elix 3 instrument). DNA oligonucleotides were purchased from Integrated DNA technologies (IDT). All enzymes for cloning and mutagenesis were obtained from Thermo Fischer Scientific. *E. coli* BL21 (DE3), BL21 (DE3) pLysS, and NEB5 $\alpha$  cells were purchased from Promega and New England Biolabs (NEB). 5-nitrobenzoxazole (5-NBI) was prepared according to the literature procedure<sup>36</sup> while 6-nitrobenzotriazole (6-NBT) was purchased from AK scientific. pET28a(+) vector was obtained from Novagen. (L)-Ascorbic acid, superoxide dismutase and catalase (from bovine liver) were obtained from Sigma Aldrich. Labeled  $^{15}\text{NH}_4\text{Cl}$  and  $^{13}\text{C}_6$ -D-glucose were purchased from Cambridge Isotope Laboratories.

### Protein expression and purification

**Myoglobin variants.**—His64 was mutated to valine (H64V) using splicing by overlap extension (SOE) PCR. At the first PCR, the combination of mutagenic primers targeting the desired site and primer pair overlapping the 5' and 3' termini of the gene generated two mutant fragments (primer sequences for two pairs of primers are shown in Supplementary Table 1: NcoI\_XhoI\_F + H64V\_R and NcoI\_XhoI\_R + H64V\_F) which served as templates

for the second PCR. Product of the second PCR was cloned into pET28a vector using *NcoI* and *XhoI* restriction sites. Mutations were introduced as needed using SOE protocol instead of site-directed mutagenesis. Myoglobin proteins contain many histidine residues (Mb-H64V has 11 His residues) and bind to the Ni-NTA column without any additional His-tag. Plasmids encoding the appropriate genes in pET28a vector were transformed into *E. coli* BL21 (DE3) and plated on LB agar with 50 µg/mL kanamycin (Kan). This concentration of antibiotic was used in all experiments. Single colonies were inoculated into LB media containing Kan and grown at 37 °C for 5–6 h. Starter culture (10 mL) was inoculated into LB (1 L) with Kan and allowed to grow at 37 °C until OD<sub>600</sub> reached 0.6–0.8. Next, δ-aminolevulinic acid (Tokyo Chemical Industry, 0.3 mM) was added and the culture was induced by the addition of 0.25 mM isopropyl-β-D-1-thiogalactopyranoside (IPTG) and grown at 25 °C for 20 h. Cells were harvested by centrifugation at 4 °C, 4,000 g, flash frozen in liquid nitrogen and stored at –80 °C. For protein purification, cells were resuspended in buffer A (25 mM TRIS, pH 8.0), lysed by sonication, and centrifuged to isolate the soluble fraction. The lysate was loaded onto a Ni-NTA column (Clontech) pre-equilibrated with buffer A, washed and eluted using a gradient of 20–250 mM imidazole in buffer A. Protein fractions were exchanged into buffer B (20 mM HEPES, pH 7.0) using desalting column. Further purification was performed on cation exchange column (HiTrap SP HP, GE Healthcare) and FPLC in buffer B using NaCl gradient of 0–600 mM (this step is absolutely critical). Eluted protein fractions were analyzed by UV-vis spectroscopy and only the fractions with the appropriate Soret band maxima (Supplementary Table 2) were exchanged into buffer B. Protein concentrations were determined from Soret band maxima using extinction coefficient of 157,000 M<sup>-1</sup>cm<sup>-1</sup> or coefficients experimentally determined using pyridine hemochromagen assay<sup>37</sup>. For the expression of the isotopically labelled proteins the plasmid was transformed into *E. coli* BL21 (DE3) cells and plated on LB agar containing Kan. Individual colonies were inoculated into LB (20 mL) with Kan and then the culture was incubated at 37 °C for 5–6 h shaking at 200 rpm. This culture was diluted with Terrific Broth (TB, 2 L) and Kan and grown at 37 °C until OD<sub>600</sub> reached 0.6–0.8. Cells were collected by centrifugation, resuspended in unlabeled M9 minimal media (18 mL) and transferred to labelled M9 minimal media (1 L) prepared with <sup>15</sup>NH<sub>4</sub>Cl and dextrose (or <sup>13</sup>C<sub>6</sub>-glucose) containing Kan and then the culture was grown at 37 °C for 3–4 h. Next, δ-aminolevulinic acid (0.3 mM) was added as heme precursor and the culture was induced by adding IPTG (0.25 mM). The culture was further grown at 25 °C for 20 h. Cells were collected by centrifugation and preserved at –80 °C. Purification was performed following the same protocol as for unlabeled protein. **AlleyCat variants.** Plasmids encoding SUMO-AlleyCat variants were transformed into *E. coli* BL21 (DE3) cells and plated on LB agar plate containing Kan. An individual colony was inoculated in LB containing Kan and grown at 37 °C for 5–6 h. 10 mL of starter culture was diluted with 1 L LB media supplemented with Kan and grown at 37 °C until OD<sub>600</sub> reached to ~ 0.6–0.8. The culture was induced by 0.5 mM IPTG and grown at 18 °C for 20 h. Cells were collected by centrifugation and resuspended in resuspension buffer (25 mM TRIS, pH 8.0, 20 mM imidazole, 10 mM CaCl<sub>2</sub>, 300 mM NaCl) with 0.5 mM phenylmethylsulfonyl fluoride. Cells were lysed by sonication (Microson) and the soluble fraction was loaded on a Ni-NTA sepharose column (HisTrap, GE Healthcare). The proteins were eluted with the buffer containing 25 mM TRIS, pH 8.0, 20 mM imidazole, 10 mM CaCl<sub>2</sub>, 300 mM NaCl and 20–500 mM imidazole applied in a

gradient fashion on a FPLC system (NGC, BioRad). After buffer exchange on a desalting column (BioRad, 10 DG) into a cleavage buffer (50 mM TRIS, pH 8.0, 75 mM NaCl), SUMO protease (at protein-to-protease absorbance ( $A_{280}$ ) ratio of 200:1) along with EDTA (Invitrogen, 0.5 mM) and DTT (Sigma, 1 mM) was added to cleave the SUMO fusion tag. After incubation at 30 °C for 3–4 h, the protein was exchanged into storage buffer (20 mM HEPES, pH 7.0, 10 mM  $\text{CaCl}_2$ , 100 mM NaCl). Protein was further purified by anion exchange chromatography (Q HP FF, GE Healthcare) in storage buffer with elution gradient of 100–800 mM NaCl. Protein fractions were exchanged into storage buffer, concentrated using 5K MWCO spin concentrator (Corning). Protein concentrations were determined by measuring the absorbance at 280 nm using a calculated extinction coefficient of 2980  $\text{M}^{-1}\text{cm}^{-1}$ . For the expression of isotopically labelled AlleyCat variants the plasmid was transformed into *E. coli* BL21 (DE3) cells and plated on LB agar plate containing Kan. Single colony was inoculated with 2 mL of LB media containing Kan and grown at 37 °C for 5–6 h, then 18 mL of unlabeled M9 minimal media with Kan was added and the culture was grown at 37 °C for an additional 5–6 h. The resulting 20 mL starter culture was diluted with 1 L of M9 media made with  $^{15}\text{NH}_4\text{Cl}$  as  $^{15}\text{N}$  and  $^{13}\text{C}_6$ -glucose, supplemented with Kan, and grown at 37 °C until  $\text{OD}_{600}$  reached to ~ 0.6–0.8. The culture was then induced by 0.5 mM IPTG and grown at 18 °C for 20 h. The cells were then harvested by centrifugation and the isotopically labeled protein was purified as discussed above. SDS-PAGE gels for all proteins used in this study are shown in Supplementary Fig. 1.

### Reduction and concentration determination of myoglobin variants

For standardization of dithionite, 20–30 mg of solid dithionite (Riedel-de Haen, Germany) as well as potassium ferricyanide (Sigma) were brought into the glovebox with a dinitrogen atmosphere (keeping oxygen under 2 ppm at all times). Both the solid reagents were dissolved in 1 mL of degassed MilliQ water to prepare stock solutions. Dithionite stock was further diluted by 20-fold. Next, two 1 mL solutions were prepared where in the first one, potassium ferricyanide stock was diluted by 100-fold while in the second one, a 1:1 mixture of ferricyanide stock and 20-fold diluted dithionite solution was prepared with subsequent dilution of each of them by 100-fold. Absorbances of both the solutions were measured at  $\lambda_{\text{max}} = 420$  nm using UV-vis diode array spectrophotometer (Agilent 8453). The reducing equivalence of 20-fold diluted dithionite solution was calculated from the difference in absorbances of the solutions using extinction coefficient of 1,020  $\text{M}^{-1}\text{cm}^{-1}$  at 420 nm. Protein concentrations were determined using the extinction coefficient of 157,000  $\text{M}^{-1}\text{cm}^{-1}$  at absorption maxima at 434 nm for reduced species. Absorbance spectra of Mb-H64V and Mb-L29I/H64G/V68A (FerreICat) in the oxidized and reduced forms are shown in Extended Data Fig. 6. It is very important to ensure that the reduced protein has a sharp peak at ~434 nm without any pronounced shoulders (both in the reduced and oxidized forms) that could be indicative of multiple protein species present.

### Kinetic characterization

In all cases the rates are corrected for the background rates in the appropriate buffers without the enzymes. Extinction coefficients of 15,800  $\text{M}^{-1}\text{cm}^{-1}$  at 380 nm was used for the product of Kemp elimination, 2-hydroxybenzoxitrile. Catalytic efficiency ( $k_{\text{cat}}/K_M$ ) as well as individual kinetic parameters ( $k_{\text{cat}}$  and  $K_M$ , where possible), were determined by

fitting the dependence of initial rates on substrate concentration (final concentration of 140–840  $\mu\text{M}$ ) to the Michaelis-Menten equation  $v_0 = k_{\text{cat}}[E][S]/(K_M+[S])$ . For proteins with high  $K_M$  values, where substrate saturation could not be achieved due to solubility limits,  $k_{\text{cat}}/K_M$  was determined by fitting data to  $v_0 = (k_{\text{cat}}/K_M)[E][S]$ . **Myoglobin mutants.** The substrate, 5-nitrobenzisoazole, was prepared as 100 mM stock in acetonitrile inside the glovebox (MBRAUN). Degassed protein samples were reduced by adding *ca.* 10 equivalents of sodium dithionite (Riedel-de Haen, Germany) inside a glovebox. Concentrations of reduced proteins were determined using the extinction coefficient of  $157,000 \text{ M}^{-1}\text{cm}^{-1}$  for the Soret band. The quality of the reduced protein was assessed by examining the position and shape of Soret and Q-bands. Protein solutions containing reduced myoglobin mutants (10 – 200 nM) in 40 mM TRIS, pH 8.0 with ascorbate (2 mM), SOD (0.2  $\mu\text{M}$ ), catalase (40 nM) introduced to suppress side reactions stemming from any dioxygen present during the measurements, were prepared inside the glovebox in glass vials. To achieve best reproducibility, it is critical to prepare the solution containing ascorbate, SOD, catalase and the reduced protein prior to **each** kinetic measurement. Ascorbate, SOD and catalase were added as separate drops to the walls of the vials, the protein was added to the buffer inside the vials, then the reagents were mixed by swirling and immediately transferred to gas-tight syringes for kinetic measurements. All measurements were done at least in triplicate, and multiple independently prepared protein batches were characterized for key mutants (FerrE1Cat, Mb-64V, Mb-64G, Mb-64G/68A). The substrate was prepared in the glove box as 2x solution in water containing 3% acetonitrile (created using appropriate volumes of 100 mM stock solution of 5-NBI in acetonitrile, water and acetonitrile to maintain the constant final concentration of co-solvent) and transferred in gas-tight syringes. Reactions were initiated by mixing reduced enzyme in buffer and solutions of 5-nitrobenzisoazole in water in 1:1 ratio on the Applied Photophysics SX20 stopped-flow spectrometer; the lines prior to the introduction of the reactants were equilibrated using deoxygenated water for the substrate channel and deoxygenated buffer in the protein channel. The final reaction mixtures contained reduced protein (5 – 100 nM) in 20 mM TRIS, pH 8.0 with ascorbate (1 mM), SOD (0.1  $\mu\text{M}$ ), catalase (20 nM), 1.5 % acetonitrile and variable concentrations of the substrate. Product formation was monitored at 25 °C for the time interval of 0.1–10 s. The corresponding kinetic parameters are given in Extended Data Table 1. The pH dependence of FerrE1Cat enzymatic activity was assessed using the protocol described above, except different buffers were used (all at 20 mM; MES at pH 6.5, HEPES at pH 7.0 and 7.5, TRIS at pH 8.0 and pH 8.5, Supplementary Fig. 3). **AlleyCat proteins.** The product formation was monitored on a BioTek Eon3 platerreader in 20 mM HEPES, pH 7.0 buffer containing 10 mM  $\text{CaCl}_2$ , 100 mM NaCl and acetonitrile (1.5% constant final concentration) at 22 °C in a 96-well plate (Greiner Cellstar). The final enzyme concentration was 100 nM. The Michaelis-Menten plots for all proteins are given in Extended Data Fig. 7. The maximum  $k_{\text{cat}}/K_M$  as well as effective  $\text{pK}_a$  of the active site residue in the pH studies of AlleyCat proteins were obtained by using the equation:  $k_{\text{cat}}/K_M = (k_{\text{cat}}/K_M)_0 + (k_{\text{cat}}/K_M)_{\text{max}} \times (10^{-\text{pK}_a}/(10^{-\text{pK}_a} + 10^{-\text{pH}}))$  (Supplementary Fig. 4 and Supplementary Table 3).

## Library design

The plasmids encoding the genes of the proteins of the AlleyCat family have been constructed as reported before.<sup>33</sup> The gene encoding sperm whale myoglobin was cloned



into pET-28a(+) (Novagen) with simultaneous introduction of the H64V mutation using standard protocols. Site-specific saturation mutagenesis targeting defined site was achieved using megaprimer PCR protocol<sup>38</sup> with primer sets (Integrated DNA Technologies) which overlapped on the 5' terminus of the randomized position, together with flanking primer (T7 forward or T7 reverse), as appropriate. Saturation mutagenesis was performed using NNK codons (where N can be any base and K represents a mixture of G and T nucleotides) that cover the 20 genetically encoded amino acids (primer sequences are shown in Supplementary Table 1). The size of PCR product was verified using agarose gel electrophoresis. DNA sample was digested with *DpnI* (New England Biolabs) at 37 °C for 10–12 h to eliminate parental clone. The digested sample was transformed into *E. coli* NEB5 $\alpha$  cells (New England Biolabs) and subsequently plated on LB agar plate containing kanamycin (50  $\mu$ g/mL). After incubation at 37 °C for 10–12 h, colonies obtained from the plate were allowed to grow in LB with Kan at 37 °C for 5–6 h. Cells were harvested, and plasmids were extracted using DNA extraction kit (Monarch, New England Biolabs). Library quality was confirmed by Sanger sequencing analysis (Genewiz, Inc.) (Supplementary Fig. 5 and Supplementary Fig. 6).

### Library screening

At least 160 independent colonies were screened for each library. Myoglobin NNK libraries were transformed into *E. coli* BL21 (DE3) pLysS cells and plated on LB agar with Kan and chloramphenicol (CHL, 34  $\mu$ g/mL). Individual colonies were inoculated into LB (200  $\mu$ L) containing Kan and CHL in 96-well plate. Cultures were incubated at 37 °C until OD<sub>600</sub> 0.6–0.8 and replica plate was generated where cultures were inoculated into LB with Kan and CHL.  $\delta$ -aminolevulinic acid (0.3 mM) as heme precursor and 0.25 mM IPTG for induction were added to the cultures and grown at 25 °C for 20 h. Cells were harvested by centrifugation. Pellets were resuspended in buffer (25 mM TRIS, pH 8.0), centrifuged again, and the supernatant was discarded. A buffer containing 25 mM TRIS, pH 8.0, 0.5% triton X was used to lyse the cells and supernatant was separated by centrifugation. Activity of the clones was tested using 96-well plates in the buffer (20 mM TRIS, pH 8.0, 1 mM ascorbate, 0.1  $\mu$ M superoxide dismutase and 20 nM catalase) by measuring absorbance at 380 nm at 22 °C on a plate reader (BioTek Eon3). The activities of clones showing large increase over the starting templates were confirmed by rescreening them in triplicate. Plasmids extracted from the colonies demonstrating improved activity were sequenced (Genewiz, Inc.) to determine the identities of beneficial mutations.

Calmodulin gene libraries were transformed into *E. coli* BL21 (DE3) pLysS cells and plated on LB agar plates containing 100  $\mu$ g/mL ampicillin and 34  $\mu$ g/mL chloramphenicol (Amp and CHL at these concentrations were used in experiments with calmodulin libraries). Single colonies were inoculated with 200  $\mu$ L of LB containing Amp and CHL in 96-well plate. After incubation for 5–6 h at 37 °C, replica plates were generated. Cultures were used to inoculate 400  $\mu$ L of Zym-5052 as autoinduction media supplemented with Amp and CHL and allowed to grow at 37 °C for 12–16 h. The cells were collected by centrifugation and the supernatant was discarded. The cells were resuspended with 25 mM TRIS, pH 8.0, 20 mM imidazole, 10 mM CaCl<sub>2</sub>, 300 mM NaCl. After clearing the lysates, pellets were lysed with a buffer containing 20 mM TRIS, pH 8.0, 10 mM CaCl<sub>2</sub>, 100 mM NaCl, 0.2%

Triton X and centrifuged to separate the lysate. Kemp elimination activity was monitored at 380 nm in the buffer containing 20 mM TRIS, pH 8.0, 10 mM CaCl<sub>2</sub> and 100 mM NaCl in 96-well plates on a BioTek Eon3 platereader at 22 °C for 10 min. The activities of clones showing large increase over the starting templates were confirmed by rescreening in them triplicate. Plasmids extracted from the colonies demonstrating improved activity were sequenced (Genewiz, Inc.) to determine the identities of beneficial mutations. The C-terminal domains of the improved variants were cloned into pET-SUMO champion vector (Invitrogen) using standard protocols for detailed protein characterization. Sequences of all newly evolved proteins are given in Extended Data Table 2.

### Gene shuffling

To quickly identify the most active variant we took the most active mutant identified in the first round of screening (H64G) and tested its performance together with the other mutations found in the first round. The same procedure was repeated on the most active double mutant (Mb-H64G/V68A) to yield FerrEICat.

### NMR spectroscopy

All NMR spectra were acquired at 298 K on a Bruker Avance III HD 800 MHz spectrometer equipped with a TCI cryoprobe. The Mb-H64V samples were prepared in 20 mM HEPES pH 7.0, the AlleyCat samples were prepared in 20 mM HEPES, pH 6.9, 10 mM CaCl<sub>2</sub>, 100 mM NaCl with 2.5 mM NaN<sub>3</sub>. All samples contained 5–10 % D<sub>2</sub>O for the lock. The assignments of backbone amide resonances were obtained from 0.7–1.0 mM U-[<sup>13</sup>C,<sup>15</sup>N] protein samples using a standard set of 3D BEST HNCACB, HN(CO)CACB, HNCO and HN(CA)CO experiments. All myoglobin samples were reduced with sodium dithionite under a nitrogen atmosphere, and the NMR tubes were flame sealed. The NMR data were processed in NMRPipe<sup>39</sup> and analyzed in CCPNMR<sup>40</sup>. The CSP experiments were performed by stepwise addition of a concentrated stock solution of 6-NBT in CH<sub>3</sub>CN to U-[<sup>15</sup>N] or U-[<sup>13</sup>C,<sup>15</sup>N] protein samples at the initial concentration of 0.2 mM. At each increment, changes in chemical shifts of the protein resonances were monitored in 2D [<sup>1</sup>H,<sup>15</sup>N] HSQC spectra. The average amide CSPs ( $\delta_{\text{avg}}$ ) were obtained at two-fold molar excess of 6-NBT as  $\delta_{\text{avg}} = (\delta_{\text{N}}^2/50 + \delta_{\text{H}}^2/2)^{0.5}$ , where  $\delta_{\text{N}}$  and  $\delta_{\text{H}}$  are the chemical shift perturbations of the amide nitrogen and proton, respectively (Supplementary Data). For each observed resonance, the Z score was calculated as  $Z = (\delta_{\text{avg}} - \mu)/\sigma$ , where  $\mu$  and  $\sigma$  are, respectively, the average and the standard deviation of  $\delta_{\text{avg}}$  values for a given CSP experiment.

The NMR titration to determine  $K_d$  values for AlleyCat and cCaM protein were performed by incremental addition of a freshly-prepared 5 mM 6-NBT solution in CH<sub>3</sub>CN to a 0.2 mM [<sup>13</sup>C,<sup>15</sup>N] protein sample. At each increment, changes in chemical shifts of the protein resonances were monitored in <sup>1</sup>H-<sup>15</sup>N HSQC spectra. The binding curves were analyzed with a two-parameter nonlinear least-squares fit using a one-site binding model corrected for the dilution effect<sup>41</sup>:  $\delta_{\text{binding}} = 0.5 \delta_0 (A - (A^2 - 4R)^{0.5})$ , where  $A = 1 + R + K_d(([\text{NBT}]_0 + R[\text{protein}]_0)/([\text{NBT}]_0[\text{protein}]_0))$  where  $\delta_{\text{binding}}$  is the chemical shift perturbation at a given [6-NBT]/[protein] ratio;  $\delta_0$  is the chemical shift perturbation at 100 % 6-NBT bound; R is the [6-NBT]/[protein] ratio at a given titration point; [protein]<sub>0</sub>

and  $[NBT]_0$  are the initial concentrations of the protein sample and the 6-NBT titrant stock solution, respectively; and  $K_d$  is the equilibrium dissociation constant (Supplementary Fig. 7).

### Crystallographic methods

Crystals of FerrE1Cat were grown by hanging drop vapor diffusion method at 20 °C upon mixing protein solution and reservoir solution (100 mM TRIS, pH 8.0, 2.4 M ammonium sulfate). Crystal screening for AlleyCat9 as well as AlleyCat10 (~ 15 mg/mL in storage buffer) were performed in 96-well plate (Violamo) using sitting drop vapor diffusion method. Crystals were further grown at 293 K using hanging drop vapor diffusion method by 1:1 mixing of protein sample and reservoir buffer containing (4S)-2-methyl-2,4-pentanediol (MPD) (47%) and TBU (2%) for AlleyCat9 while 50% MPD was used for AlleyCat10. Protein samples were mixed with 6-NBT (5–10 mM), incubated on ice for 30 min and grown further following the same condition as mentioned above for co-crystallization. X-ray diffraction data were collected using a Pilatus-200 K detector on a Rigaku Micromax-007 rotating anode X-ray generator. The protein was crystallized in hexagonal space group (P6). Diffraction data were processed with the CrysAlisPro software suite (Rigaku). All structures were determined by molecular replacement using PHASER<sup>42</sup> starting with the deposited model of myoglobin (PDB code 1mbn) or AlleyCat (PDB code 2kz2). Refinement was performed by COOT<sup>43</sup> and PHENIX<sup>44</sup>, and the final structures were validated with MolProbity<sup>45</sup>. Crystallographic data and refinement statistics are given in Extended Data Table 3.

### Computational docking

5-NBI was docked into FerrE1Cat with AutoDock Vina<sup>46</sup> with previously described protocol<sup>47</sup>. The imidazole molecule coordinated to the iron in the crystal structure was removed prior to docking.

### Circular dichroism (CD) spectroscopy

All CD spectra of myoglobin variants were recorded using Jasco J-715 CD spectrometer in continuous mode with 1 nm bandwidth, 2 nm data pitch, scan rate of 50 nm/min with 8 s averaging time. The final spectra represent a buffer-subtracted average of three runs. The CD spectra of non-reduced proteins in the far-UV region (200–260 nm) were collected using quartz cuvette with 1 mm pathlength while for the Soret band region (390–470 nm) quartz cuvette of 1 cm pathlength was used. The spectra at Soret band region (390–470 nm) were obtained to determine mean residue ellipticity values (MRE) assuming protein binds heme in a 1:1 ratio. Protein stocks were diluted in 2 mM TRIS (pH 8.0) to 5  $\mu$ M and the spectra were recorded for oxidized protein. For the analysis of the reduced protein, the stock was diluted in the same way as for the oxidized sample and ten equivalents of sodium dithionite were added to the protein inside the glovebox. The concentration of the reduced protein was calculated based on the Soret band maxima using the corresponding extinction coefficients. Sample absorbance never exceeded 2 at all wavelengths. The mean residue ellipticity (MRE,  $\text{deg}\cdot\text{cm}^2\cdot\text{dmol}^{-1}$ ) values were calculated using the following equation ( $\text{MRE} = \theta/(10\cdot c\cdot l\cdot N)$ ), where  $\theta$  (mdeg) is ellipticity,  $l$  (cm) is the pathlength of the cuvette,  $c$  (M) is the protein concentration and  $N$  is the number of residues (Supplementary Fig. 8).

Chemical denaturation studies on AlleyCat proteins were performed by monitoring sample monitoring sample absorbance at 222 nm in presence of varying concentration of guanidine hydrochloride (0–6 M) as the denaturant (Supplementary Fig. 9) and thermodynamic parameters for protein unfolding were determined (Supplementary Table 4).

### **Spectroelectrochemical determination of redox potential of myoglobin mutants**

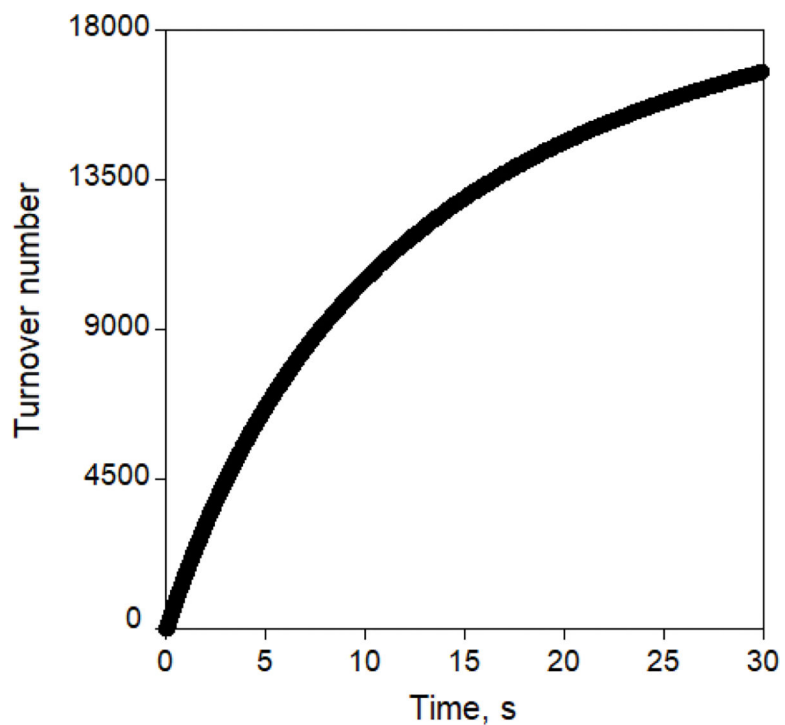
The redox potentials of myoglobin variants were measured using a platinum honeycomb spectrochemical electrode (0.17 cm) with a Ag/AgCl reference electrode connected to the WaveNow potentiostat (Pine Research Instrumentation). All redox potential were determined against Ag/AgCl reference electrode (reported as +199 mV vs NHE by manufacturer). The redox titration was performed using 1.2 mL of working solution containing ~ 20  $\mu$ M protein and 100  $\mu$ M phenazine methosulfate (Sigma) as a redox mediator in 20 mM HEPES (pH 7.0) or 20 mM TRIS (pH 8.0). A highly positive potential of +100 mV vs Ag/AgCl reference electrode was initially applied to ensure complete oxidation of protein. Next, the potential was applied with an increment of 25 mV from +25 mV to –500 mV (vs Ag/AgCl) with the equilibration time of 5 min at 20 °C for each step. The absorbance spectra of the protein containing mixtures at each potential were recorded using UV-vis spectrophotometer (Agilent 8453). The absorbance of the protein solution was corrected for the contribution of the mediator. The absorbance at 434 nm was normalized to 800 nm and used to determine the fraction of reduced protein in the sample using the equation (Fraction reduced =  $(A_{434} - A_{434, \text{min}})/(A_{434, \text{max}} - A_{434, \text{min}})$ ). Fraction reduced was plotted as a function of the applied potential and the midpoint reduction potential ( $E_m$ ) was determined using the following equation: Fraction reduced =  $(A + g*x)/(1 + (x/E_m)^b)$ , where A is fraction reduced at complete reduction, x is applied potential,  $E_m$  is midpoint reduction potential, b is a slope of the linear portion of a sigmoidal curve and g is the slope of the top linear portion of the curve. The midpoint reduction potentials obtained from the fits (Extended Data Fig. 4) are summarized in Supplementary Table 5.

### **Determination of the dissociation constants for AlleyCats and 6-nitrobenzotriazole (inhibitor).**

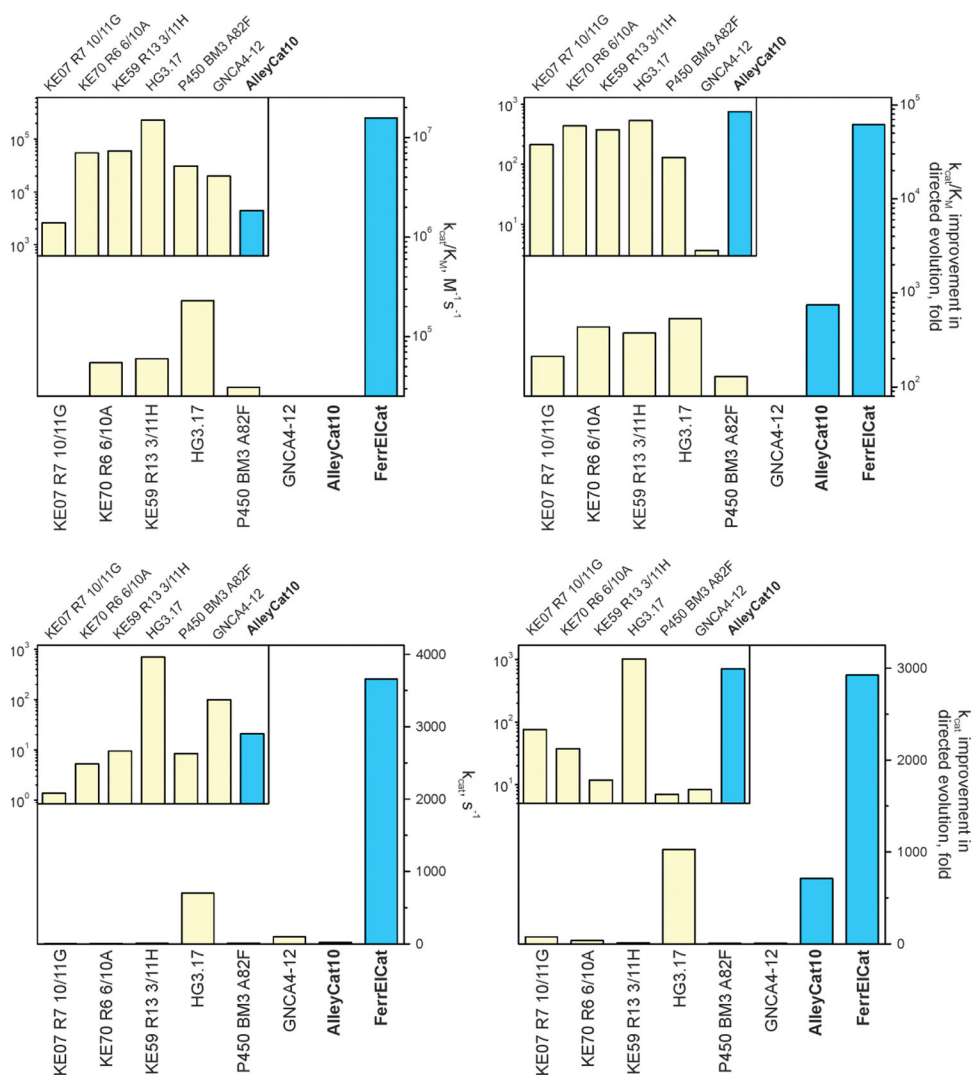
The thermodynamic parameters of 6-nitrobenzotriazole (6-NBT) binding to AlleyCat proteins were measured using a MicroCal PEAQ-ITC instrument (Malvern Panalytical). Proteins were dialyzed against buffer (20 mM HEPES, 100 mM NaCl, 10 mM CaCl<sub>2</sub>, pH 7.0) containing 2% acetonitrile, filtered using 0.22  $\mu$ m low protein binding PES filter (Santa Cruz Biotechnology, Inc.) and the concentration of each sample was determined by UV-vis spectroscopy using extinction coefficients of 2,980 M<sup>-1</sup>cm<sup>-1</sup> at 280 nm. 6-NBT was prepared by dissolving the powder in the protein dialysis buffer to obtain 1 mM solution. All titrations were performed at 25 °C in the high feedback mode with 750 rpm stir speed and an appropriate equilibration time between injections (150 s). The protein sample (~100  $\mu$ M) was placed in the calorimeter cell and 1 mM solution of 6-NBT (in the syringe) was added to the protein in eighteen 2  $\mu$ L aliquots. As a control, 1 mM 6-NBT solution was titrated into the dialysis buffer.

The analysis, including baseline correction, peak integration and correction for heat of dilution observed at the protein saturation with inhibitor, was performed using the MicroCal



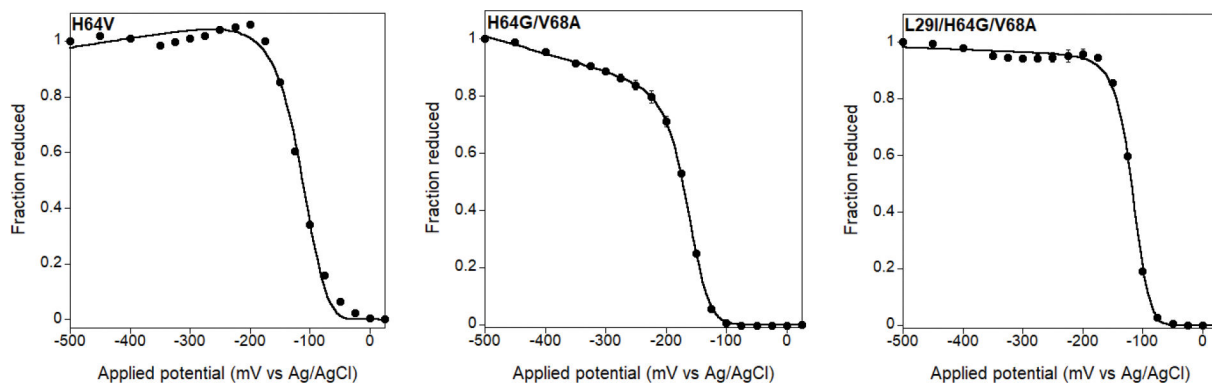


**Extended Data Fig. 2 |** Substrate turnover by reduced Mb-L29I/H64G/V68A (FerrEIcat). Reaction was monitored using stopped-flow at pH 8.0 for 30 s at 25 °C with 140  $\mu$ M of 5-NBI and 5 nM of FerrEIcat.



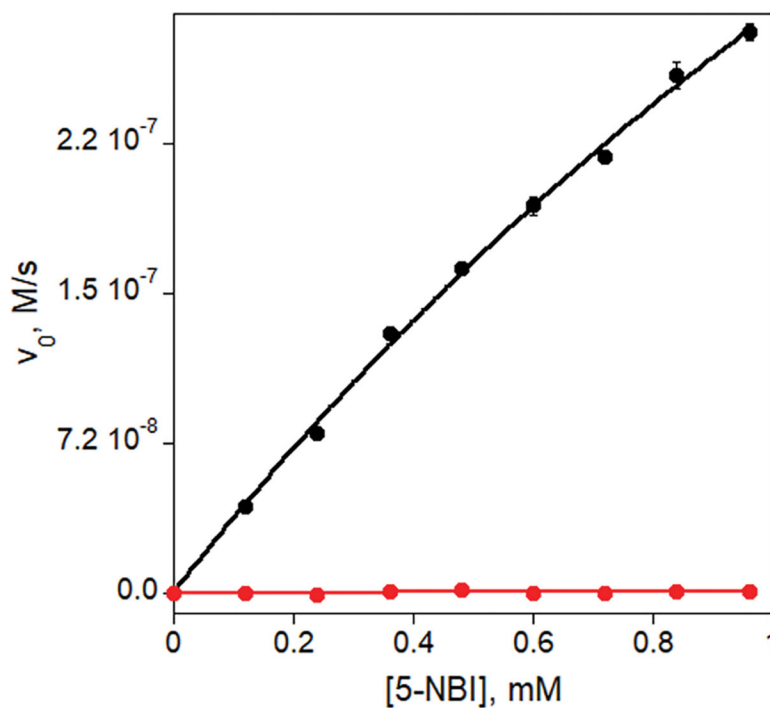
**Extended Data Fig. 3 | Catalytic parameters of Kemp eliminases evolved using directed evolution:**

$k_{cat}/K_M$  and  $k_{cat}$  values for the evolved enzymes (left) and improvement in  $k_{cat}/K_M$  and  $k_{cat}$  achieved by directed evolution (right). In cases where only  $k_{cat}/K_M$  was reported, we used 5 mM for  $K_M$ , to obtain low estimate of the  $k_{cat}$ .



**Extended Data Fig. 4 | Spectroelectrochemical determination of redox potentials of selected myoglobin mutants.**

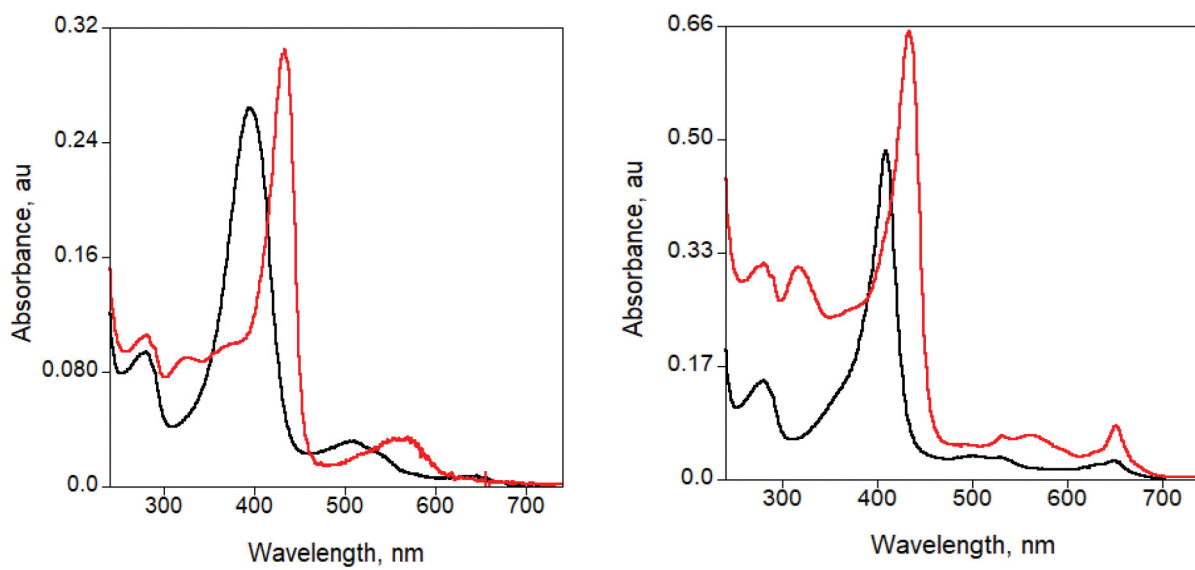
The proteins were analyzed in 20 mM TRIS-HCl (pH 8.0) at 20 °C in presence of the mediator (100  $\mu$ M phenazine sulfate). The redox potentials (vs Ag/AgCl) are summarized in Supplementary Table 5.



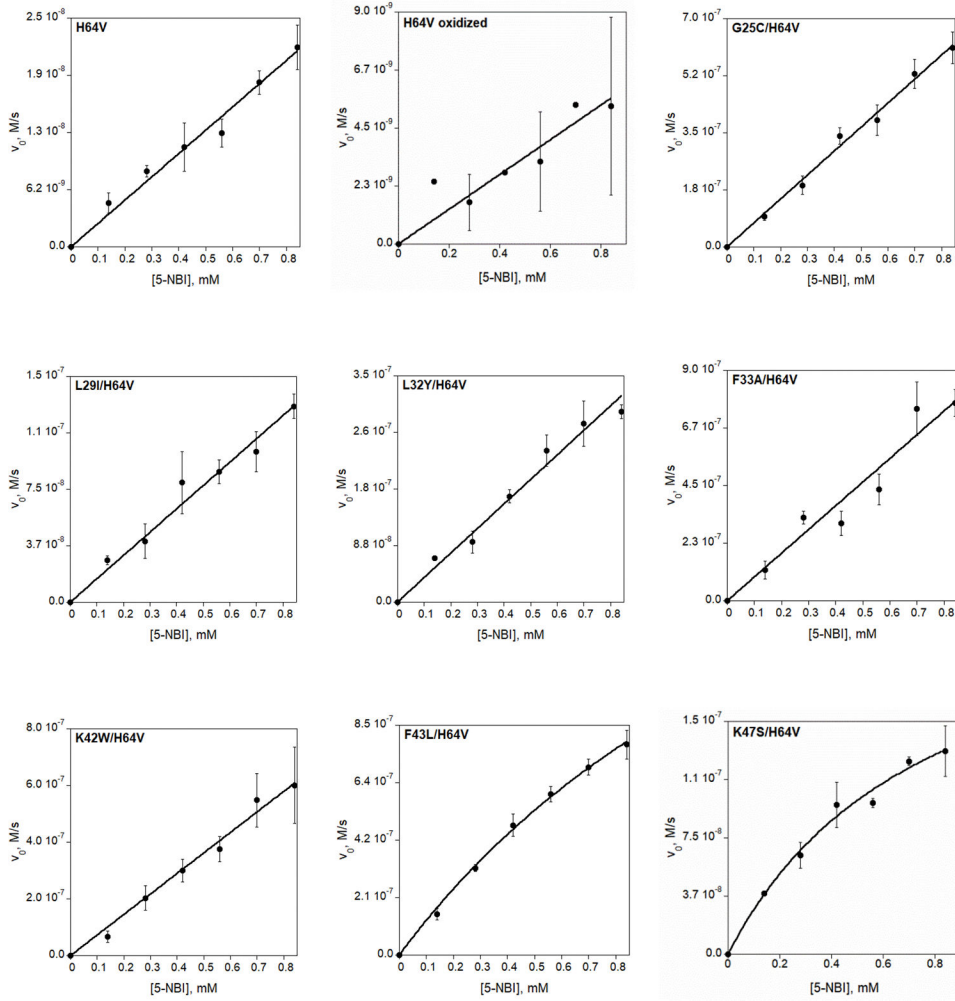
**Extended Data Fig. 5 | Kemp elimination catalyzed by AlleyCat10 in presence of  $\text{Ca}^{2+}$  (black) and in absence of  $\text{Ca}^{2+}$  (red).**

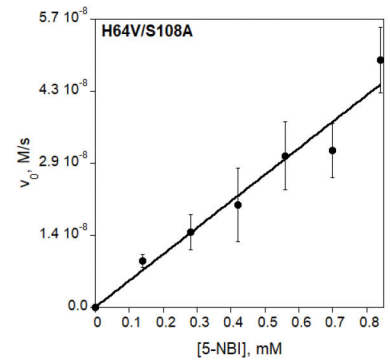
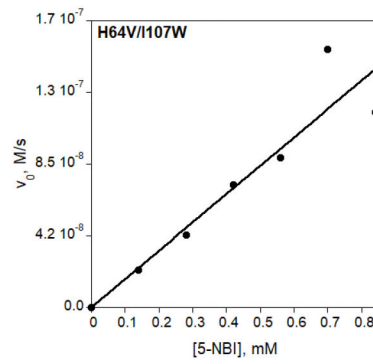
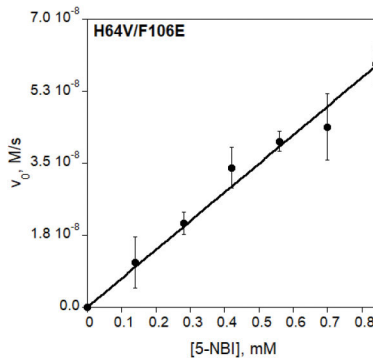
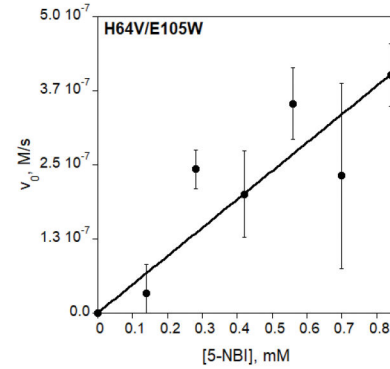
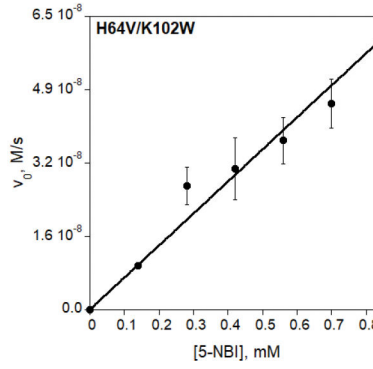
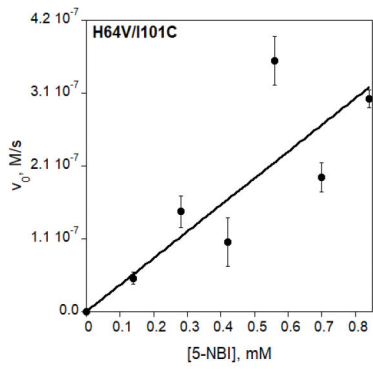
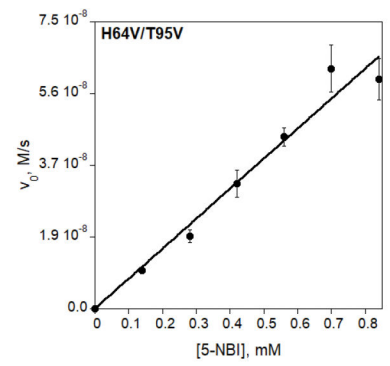
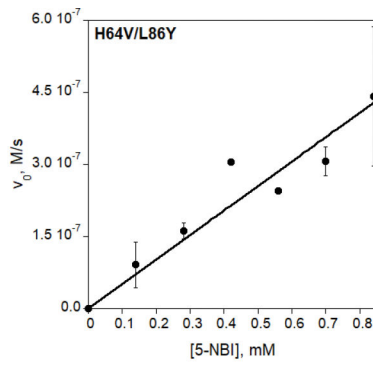
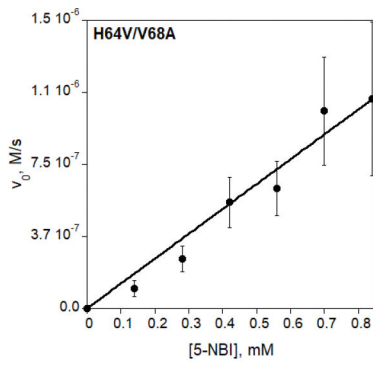
The activity of 0.1  $\mu$ M AlleyCat10 was tested with 0.12–0.96 mM substrate in 20 mM HEPES, 100 mM NaCl (pH 7.0) at 22°C with 10 mM  $\text{CaCl}_2$  (black) or 100  $\mu$ M EDTA (red).

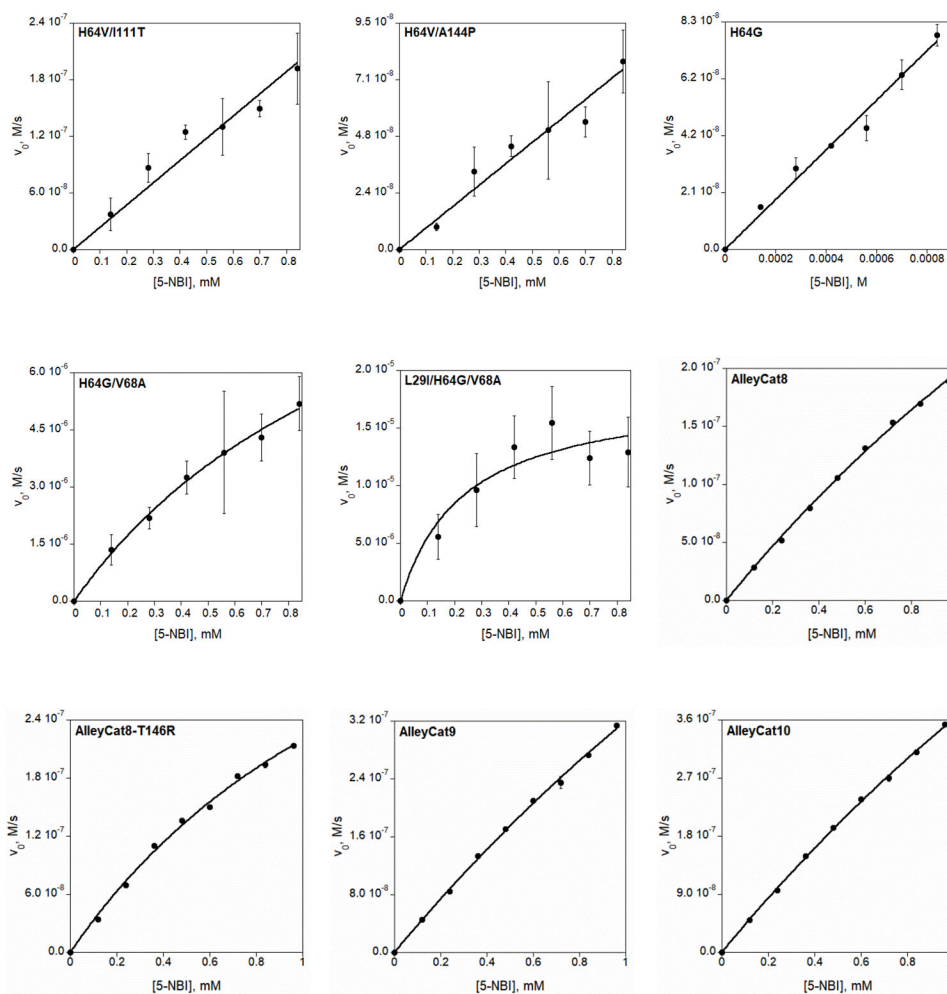




**Extended Data Fig. 6 |.** Absorbance spectra of Mb-H64V (left) and Mb-L29I/H64G/V68A (FerrEIcat) (right) in the oxidized (black) and reduced (red) forms.







**Extended Data Fig. 7 | Michaelis-Menten plots of Kemp elimination catalyzed by reduced (unless otherwise stated) myoglobin mutants and by AlleyCat proteins.**

Final reaction mixtures for myoglobin mutant analyses contained 1 mM L-ascorbic acid, 0.1  $\mu\text{M}$  SOD, 20 nM catalase, 140–840  $\mu\text{M}$  substrate, 1.5% acetonitrile in 20 mM TRIS (pH 8.0). The protein concentration was 1  $\mu\text{M}$  for Mb-H64V, 0.1 or 0.25  $\mu\text{M}$  for Mb-H64V-based double variants, 5 nM for Mb-H64G or Mb-H64G-based double or triple variants. AlleyCat reaction mixtures contained 0.1  $\mu\text{M}$  proteins with 0.12–0.96 mM substrate in 1.5% acetonitrile, 20 mM TRIS (pH 8.0), 10 mM  $\text{CaCl}_2$ , 100 mM NaCl. Kinetic parameters are summarized in Table 1 and Extended Data Table 1.

**Extended Data Table 1 |**

Kinetic parameters for the Kemp elimination reaction catalyzed by myoglobin variants in the reduced state (unless otherwise stated).

Protein	$k_{\text{cat}}$ , $\text{s}^{-1}$	$K_M$ , mM	$k_{\text{cat}}/K_M$ , $\text{M}^{-1}\text{s}^{-1}$
H64V	–	–	$255 \pm 8$
H64V (oxidized)	–	–	$7 \pm 1$

Protein	$k_{cat}$ , $s^{-1}$	$K_M$ , mM	$k_{cat}/K_M$ , $M^{-1}s^{-1}$
G25C/H64V	–	–	7,354 ± 143
L29I/H64V	–	–	1,550 ± 55
L32Y/H64V	–	–	3,795 ± 122
F33A/H64V	–	–	9,270 ± 523
K42W/H64V	–	–	7,237 ± 192
F43L/H64V	26.10 ± 3.85	1.94 ± 0.38	13,458 ± 670
K47S/H64V	2.55 ± 0.39	0.79 ± 0.21	3,240 ± 994
H64V/V68A	–	–	12,939 ± 622
H64V/L86Y	–	–	5,097 ± 355
H64V/T95V	–	–	785 ± 32
H64V/I101C	–	–	3,844 ± 551
H64V/K102W	–	–	710 ± 28
H64V/E105W	–	–	4,786 ± 538
H64V/F106E	–	–	697 ± 22
H64V/I107W	–	–	1,680 ± 135
H64V/S108A	–	–	524 ± 24
H64V/I111T	–	–	2,356 ± 114
H64V/A144P	–	–	900 ± 43
H64G	–	–	18,152 ± 519
H64G/V68A	2,557 ± 372	1.28 ± 0.28	1,992,300 ± 143,420
L29I/H64G/V68A	3,656 ± 667	0.23 ± 0.13	15,721,000 ± 6,035,800

### Extended Data Table 2 |

Sequences of the proteins used in this study.

Protein	Sequence			
<b>Mb-H64V</b>	MVLSEGEWQL	VLHVWAKVEA	DVAGHGQDIL	IRLFKSHPET
	LEKFDRFKHL	KTEAEMKASE	DLKKVGVTVL	TALGAILKKK
	GHHEAELKPL	AQSHATKHKI	PIKYLEFISE	AIHVLHSRH
	PGNFGADAQG	AMNKALELFR	KDIAAKYKEL	GYQG
<b>FerrEICat</b>	MVLSEGEWQL	VLHVWAKVEA	DVAGHGQDII	IRLFKSHPET
	LEKFDRFKHL	KTEAEMKASE	DLKKGGVTAL	TALGAILKKK
	GHHEAELKPL	AQSHATKHKI	PIKYLEFISE	AIHVLHSRH
	PGNFGADAQG	AMNKALELFR	KDIAAKYKEL	GYQG
<b>AlleyCat</b>	MKDTDSEEEI	REAFRVEDKD	NGYISAAEL	RHVMTNLGEK
	LTDEEVDEMI	READIDGDGQ	VNYEEFVQMM	TAK
<b>AlleyCat7</b>	MKDTDSEEEI	REQFRVEDKD	NGYISAAEL	RIVMTNRGEK
	LTDEEVDELI	RETDIDGDGQ	VNYEEFVQRM	TAK
<b>AlleyCat8</b>	MKDTDSEEEI	REQFRVEDKD	NGYISAAEL	RIVMTNRGEK
	LTDEEVDELH	RETDIDGDGQ	VNYEEFVQRM	TAK
<b>AlleyCat8-T146R</b>	MKDTDSEEEI	REQFRVEDKD	NGYISAAEL	RIVMTNRGEK

Protein	Sequence			
		LTDEEVDELH	RETDIDGDGQ	VNYEEFVQRM
AlleyCat9	MKDTDSEEL	REQFRVEDKD	GNGYISAAEL	RIVMTNRGEP
	LTDEEVDELH	RETDIDGDGQ	VNYEEFVQRM	TAK
AlleyCat10	MKDTDSEEL	REQFRVEDKD	GNGYISAAEL	RIVMTNRGEP
	LTDEEVDELH	RETDIDGDGQ	VNYEEFVQRM	PAK

### Extended Data Table 3 |

Crystallographic data collection and refinement statistics.

	FerrElCat	AC9	AC9_6-NBT	AC10	AC10_6-NBT
<b>Data collection</b>					
Space group	P6	P212121	P43212	P212121	P43212
Cell dimensions					
<i>a, b, c</i> (Å)	90.02, 90.02,45.37	27.38, 58.71, 87.51	82.97,82.97, 104.07	27.31,50.50, 88.25	82.92, 82.92,104.95
<i>α, β, γ</i> °	90.00, 90.00, 120.00	90.00, 90.00,120.00	90.00,90.00,90.00	90.00,90.00, 90.00	90.00,90.00,90.00
Resolution (Å)	22.68– 1.40(1.42– 1.40)	12.75– 1.70(1.73– 1.70)*	12.98–1.70(1.73– 1.70)*	12.50– 1.70(1.73– 1.70)*	13.19–1.95 (2.02– 1.95)*
<i>R<sub>sym</sub></i> or <i>R<sub>merge</sub></i>		0.072	0.095	0.081	0.153
<i>I</i> / <i>σI</i>	15.5	13.6	15.8	10.0	11.2
Completeness (%)	99.8	99.3	99.7	99.5	99.7
Redundancy	6.9	4.9	9.8	4.5	10.6
<b>Refinement</b>					
Resolution (Å)	22.68–1.40	12.75–1.70	12.98–1.70	12.75–1.70	13.19–1.95
No. reflections	286602	16079	40502	13978	27277
<i>R<sub>work</sub></i> / <i>R<sub>free</sub></i>	17.7/19.5	17.9/21.4	21.4/25.2	19.7/24.5	24.9 / 27.8
No. atoms	1501	1181	4288	1221	2261
Protein	1218	1068	4030	1084	2114
Ligand/ion		5	64/15	6	48/17
Water	231	92	135	131	82
<i>B</i> -factors	12.0	12.0	20.3	12.0	16.0
Protein	10.7				
Ligand/ion					
Water	22.0				
R.m.s. deviations					
Bond lengths (Å)	0.005	0.006	0.009	0.006	0.006
Bond angles (°)	0.772	0.819	0.819	0.741	0.763

\* Values in parentheses are for highest-resolution shell.

## Supplementary Material

Refer to Web version on PubMed Central for supplementary material.

## Acknowledgments

This work was supported by the National Institutes of Health grant (grant no. GM119634) and the Alexander von Humboldt Foundation. The authors thank Prof. Rudi Fasan for the gift of the plasmid containing the Mb gene. J.R.H.T. thanks OpenEye Scientific Software.

## References

1. Bornscheuer UT et al. Engineering the third wave of biocatalysis. *Nature* 485, 185–194 (2012). [PubMed: 22575958]
2. Reetz MT Laboratory evolution of stereoselective enzymes: a prolific source of catalysts for asymmetric reactions. *Angew. Chem. Int. Ed. Engl.* 50, 138–174 (2011). [PubMed: 20715024]
3. Denard CA, Ren H & Zhao H Improving and repurposing biocatalysts via directed evolution. *Curr. Opin. Chem. Biol.* 25, 55–64 (2015). [PubMed: 25579451]
4. Chen K & Arnold FH Engineering new catalytic activities in enzymes. *Nat. Catal* 3, 203–213 (2020).
5. Reetz MT, Wilensek S, Zha D & Jaeger KE Directed evolution of an enantioselective enzyme through combinatorial multiple-cassette mutagenesis. *Angew. Chem. Int. Ed. Engl.* 40, 3589–3591 (2001). [PubMed: 11592190]
6. Wijma HJ, Floor RJ & Janssen DB Structure- and sequence-analysis inspired engineering of proteins for enhanced thermostability. *Curr. Opin. Struct. Biol.* 23, 588–594 (2013). [PubMed: 23683520]
7. Planas-Iglesias J et al. Computational design of enzymes for biotechnological applications. *Biotechnol. Adv.* 47, 107696 (2021). [PubMed: 33513434]
8. Verma R, Schwaneberg U & Roccatano D Computer-aided protein directed evolution: a review of web servers, databases and other computational tools for protein engineering. *Comput. Struct. Biotechnol. J.* 2, e201209008 (2012). [PubMed: 24688649]
9. Ebert MC & Pelletier JN Computational tools for enzyme improvement: why everyone can - and should - use them. *Curr. Opin. Chem. Biol.* 37, 89–96 (2017). [PubMed: 28231515]
10. Osuna S The challenge of predicting distal active site mutations in computational enzyme design. *WIREs Comput. Mol. Sci.* 11, e1502 (2021).
11. Wu Z, Kan SBJ, Lewis RD, Wittmann BJ & Arnold FH Machine learning-assisted directed protein evolution with combinatorial libraries. *Proc. Natl. Acad. Sci. U.S.A.* 116, 8852–8858 (2019). [PubMed: 30979809]
12. Acevedo-Rocha CG et al. Pervasive cooperative mutational effects on multiple catalytic enzyme traits emerge via long-range conformational dynamics. *Nat. Commun.* 12, 1621 (2021). [PubMed: 33712579]
13. Otten R et al. How directed evolution reshapes the energy landscape in an enzyme to boost catalysis. *Science* 370, 1442–1446 (2020). [PubMed: 33214289]
14. Campbell E et al. The role of protein dynamics in the evolution of new enzyme function. *Nat. Chem. Biol.* 12, 944–950 (2016). [PubMed: 27618189]
15. Hong NS et al. The evolution of multiple active site configurations in a designed enzyme. *Nat. Commun.* 9, 3900 (2018). [PubMed: 30254369]
16. Broom A et al. Ensemble-based enzyme design can recapitulate the effects of laboratory directed evolution in silico. *Nat. Commun.* 11, 4808 (2020). [PubMed: 32968058]
17. Warshel A et al. Electrostatic basis for enzyme catalysis. *Chem. Rev.* 106, 3210–3235 (2006). [PubMed: 16895325]
18. Kemp DS & Casey ML Physical organic chemistry of benzisoxazoles. II. Linearity of the Bronsted free energy relationship for the base-catalyzed decomposition of benzisoxazoles. *J. Am. Chem. Soc.* 95, 6670–6680 (1973).
19. Rothlisberger D et al. Kemp elimination catalysts by computational enzyme design. *Nature* 453, 190–195 (2008). [PubMed: 18354394]
20. Blomberg R et al. Precision is essential for efficient catalysis in an evolved Kemp eliminase. *Nature* 503, 418–421 (2013). [PubMed: 24132235]

21. Risso VA et al. *De novo* active sites for resurrected Precambrian enzymes. *Nat. Commun.* 8, 16113 (2017). [PubMed: 28719578]
22. Merski M & Shoichet BK Engineering a model protein cavity to catalyze the Kemp elimination. *Proc. Natl. Acad. Sci. U.S.A.* 109, 16179–16183 (2012). [PubMed: 22988064]
23. Debler EW, Muller R, Hilvert D & Wilson IA An aspartate and a water molecule mediate efficient acid-base catalysis in a tailored antibody pocket. *Proc. Natl. Acad. Sci. U.S.A.* 106, 18539–18544 (2009). [PubMed: 19846764]
24. Vaissier V, Sharma SC, Schaettle K, Zhang T & Head-Gordon T Computational optimization of electric fields for improving catalysis of a designed Kemp eliminase. *ACS Catal.* 8, 219–227 (2018).
25. Lamba V et al. Kemp eliminase activity of ketosteroid isomerase. *Biochemistry* 56, 582–591 (2017). [PubMed: 28045505]
26. Risso VA et al. Enhancing a *de novo* enzyme activity by computationally-focused ultra-low-throughput screening. *Chem. Sci.* 11, 6134–6148 (2020). [PubMed: 32832059]
27. Li A et al. A redox-mediated Kemp eliminase. *Nat. Commun.* 8, 14876 (2017). [PubMed: 28348375]
28. Miao Y, Metzner R & Asano Y Kemp elimination catalyzed by naturally occurring aldoxime dehydratases. *ChemBioChem* 18, 451–454 (2017). [PubMed: 28120515]
29. Bordeaux M, Tyagi V & Fasan R Highly diastereoselective and enantioselective olefin cyclopropanation using engineered myoglobin-based catalysts. *Angew. Chem. Int. Ed. Engl.* 54, 1744–1748 (2015). [PubMed: 25538035]
30. Yi J, Heinecke J, Tan H, Ford PC & Richter-Addo GB The distal pocket histidine residue in horse heart myoglobin directs the O-binding mode of nitrite to the heme iron. *J. Am. Chem. Soc.* 131, 18119–18128 (2009). [PubMed: 19924902]
31. Wang B et al. Nitrosyl myoglobins and their nitrite precursors: crystal structural and quantum mechanics and molecular mechanics theoretical investigations of preferred Fe-NO ligand orientations in myoglobin distal pockets. *Biochemistry* 57, 4788–4802 (2018). [PubMed: 29999305]
32. Korendovych IV et al. Design of a switchable eliminase. *Proc. Natl. Acad. Sci. U.S.A.* 108, 6823–6827 (2011). [PubMed: 21482808]
33. Moroz OV et al. A single mutation in a regulatory protein produces evolvable allosterically regulated catalyst of nonnatural reaction. *Angew. Chem. Int. Ed. Engl.* 52, 6246–6249 (2013). [PubMed: 23630096]
34. Chattopadhyaya R, Meador WE, Means AR & Quiocho FA Calmodulin structure refined at 1.7 Å resolution. *J. Mol. Biol.* 228, 1177–1192 (1992). [PubMed: 1474585]
35. Marshall LR, Zozulia O, Lengyel-Zhand Z & Korendovych IV Minimalist *de novo* design of protein catalysts. *ACS Catal.* 9, 9265–9275 (2019). [PubMed: 34094654]

## Methods references

36. Casey ML, Kemp DS, Paul KG & Cox DD Physical organic chemistry of benzisoxazoles. I. Mechanism of base-catalyzed decomposition of benzisoxazoles. *J. Org. Chem.* 38, 2294–2301 (1973).
37. Berry EA & Trumppower BL Simultaneous determination of hemes a, hemes b, and hemes c from pyridine hemochrome spectra. *Anal. Biochem.* 161, 1–15 (1987). [PubMed: 3578775]
38. Barik S Megaprimer PCR. in *PCR Cloning Protocols* (eds. Chen B-Y & Janes H) 189–196 (Humana Press, Totowa, 2002).
39. Delaglio F et al. NMRPipe - a multidimensional spectral processing system based on UNIX Pipes. *J. Biomol. NMR* 6, 277–293 (1995). [PubMed: 8520220]
40. Vranken WF et al. The CCPN data model for NMR spectroscopy: development of a software pipeline. *Proteins* 59, 687–696 (2005). [PubMed: 15815974]
41. Kannt A, Young S & Bendall DS The role of acidic residues of plastocyanin in its interaction with cytochrome f. *Biochim. Biophys. Acta - Bioenerg.* 1277, 115–126 (1996).



42. Storoni LC, McCoy AJ & Read RJ Likelihood-enhanced fast rotation functions. *Acta Crystallogr. D: Struct. Biol.* 60, 432–438 (2004).
43. Emsley P, Lohkamp B, Scott WG & Cowtan K Features and development of Coot. *Acta Crystallogr. D: Biol. Crystallogr* 66, 486–501 (2010). [PubMed: 20383002]
44. Adams PD et al. PHENIX: a comprehensive Python-based system for macromolecular structure solution. *Acta Crystallogr. D: Biol. Crystallogr* 66, 213–221 (2010). [PubMed: 20124702]
45. Chen VB et al. MolProbity: all-atom structure validation for macromolecular crystallography. *Acta Crystallogr. D: Biol. Crystallogr* 66, 12–21, (2010). [PubMed: 20057044]
46. Trott O & Olson AJ AutoDock Vina: improving the speed and accuracy of docking with a new scoring function, efficient optimization and multithreading. *J. Comput. Chem.* 31, 455–461 (2010). [PubMed: 19499576]
47. Makhlynets OV & Korendovych IV Minimalist design of allosterically regulated protein catalysts. *Meth. Enzymol.* 580, 191–202 (2016).

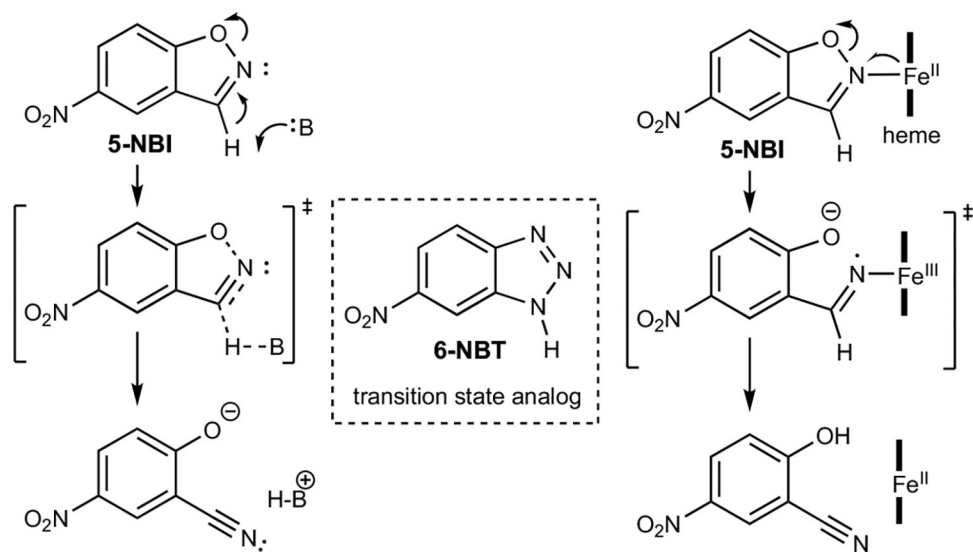
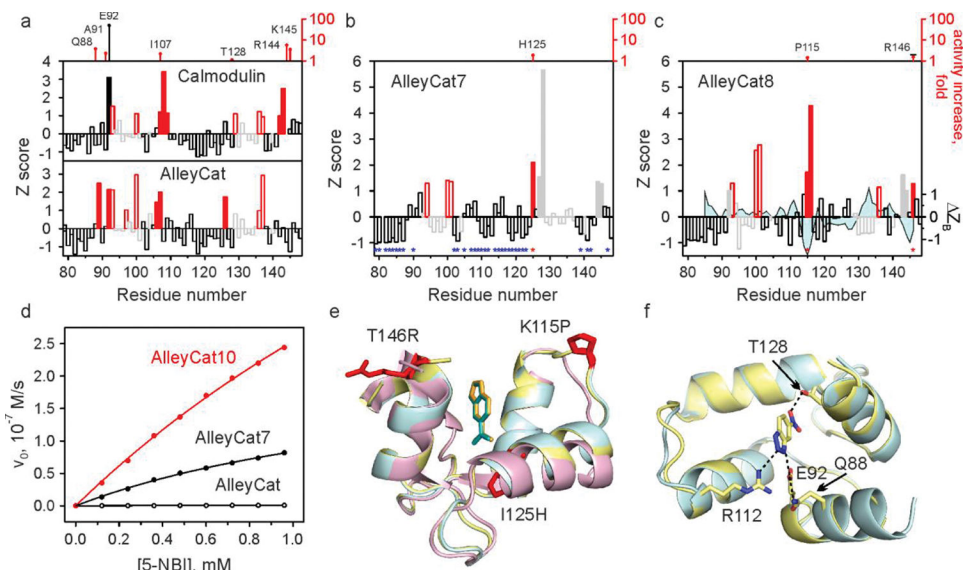


Fig. 1 | Kemp elimination promoted by acid-base or redox mechanisms.





**Fig. 3 | NMR-guided evolution of calmodulin.**

**a-c**, Backbone amide CSP of cCaM/AlleyCat (**a**), AlleyCat7 (**b**) and AlleyCat8 (**c**) upon addition of 2 molar equivalents of 6-NBT. The red bars indicate the protein regions experiencing large chemical shift perturbation ( $Z \geq 1$ ). The open red and grey bars identify EF hand residues. The catalytic F92E mutation is shown with a solid black bar. The positions where productive mutations were found are marked by red asterisks in **b** and **c** (along with the corresponding increase in  $k_{cat}/K_M$  relative to the previous round of design, top). Positions where screening identified no productive mutations are marked by blue asterisks in **b**. The solid grey bars in **b** and **c** refer to residues already mutated in previous rounds. The difference in Z-score of crystallographic B-factors ( $C\alpha$ ) for the inhibitor bound and free AlleyCat9 is mapped onto the CSP data on AlleyCat8 ( $Z_B$  trace in **c**). **d** Michaelis-Menten plots for representative proteins. **e** Overlay of the crystal structures of C-terminal domain of calmodulin (magenta), AlleyCat9 with the inhibitor (cyan) and AlleyCat10 with the inhibitor (yellow). The residues identified in CSP analysis are shown in red. **f** Overlay of the crystal structures of apo (cyan) and the inhibitor bound (yellow) in AlleyCat10.

**Table 1 |**

Kinetic parameters for Kemp elimination promoted by selected Kemp eliminases at pH 8.0. The myoglobin mutants were reduced unless stated otherwise.

Protein	$k_{\text{cat}}$ , s <sup>-1</sup>	$K_{\text{M}}$ , mM	$k_{\text{cat}}/K_{\text{M}}$ , M <sup>-1</sup> s <sup>-1</sup>
Mb-H64V <sup>a</sup>	–	–	$7 \pm 1^b$
Mb-H64V	–	–	$255 \pm 8^b$
Mb-H64V/F43L	$26.10 \pm 3.85$	$1.94 \pm 0.38$	$13,458 \pm 670$
Mb-H64V/V68A	–	–	$12,939 \pm 622^b$
Mb-H64V/L29I	–	–	$1,550 \pm 55^b$
Mb-H64G	–	–	$18,152 \pm 519^b$
Mb-H64G/V68A	$2,557 \pm 372$	$1.28 \pm 0.28$	$1,992,300 \pm 143,420$
FerrE1Cat (Mb-L29I/H64G/V68A)	$3,656 \pm 667$	$0.23 \pm 0.13$	$15,721,000 \pm 6,035,800$
AlleyCat	–	–	$5.8 \pm 0.3^{bc}$
AlleyCat7	$3.2 \pm 0.2^c$	$2.4 \pm 0.2^c$	$1283 \pm 13^c$
AlleyCat8	$10.1 \pm 1.5$	$4.1 \pm 0.7$	$2451 \pm 15$ $2369 \pm 99^d$
AlleyCat8-T146R	$5.8 \pm 0.7$	$1.6 \pm 0.3$	$3563 \pm 39$
AlleyCat9	$18.9 \pm 3.9$	$4.9 \pm 1.2$	$3857 \pm 27$ $3894 \pm 61^d$
AlleyCat10	$21.2 \pm 2.8$	$4.8 \pm 0.7$	$4378 \pm 20$ $4392 \pm 83^d$

<sup>a</sup>Oxidized form.

<sup>b</sup>Individual  $k_{\text{cat}}$  and  $K_{\text{M}}$  values could not be determined due to substrate solubility.

<sup>c</sup>from ref.<sup>31</sup>.

<sup>d</sup>( $k_{\text{cat}}/K_{\text{M}}$ )<sub>max</sub> values were obtained from the pH activity profiles.